INT. J. REMOTE SENSING, 2001, VOL. 22, NO. 8, 1479–1493

Land-cover classification methods for multi-year AVHRR data

S. LIANG

Laboratory for Global Remote Sensing Studies, Department of Geography, University of Maryland, College Park, Maryland 20742, USA; e-mail: sliang@geog.umd.edu

(*Received 28 April 1998; in final form 4 October 1999*)

Abstract. Advanced Very High Resolution Radiometer (AVHRR) data have been extensively used for global land-cover classification, but few studies have taken direct and full advantage of the multi-year properties of AVHRR data. This study focused on generating effective classification features from multi-year AVHRR data to improve classification accuracy. Three types of features were derived from 12-year monthly composite normalized difference vegetation index (NDVI) and channel 4 brightness temperature from the NOAA/NASA Pathfinder AVHRR Land data for land-cover classification. The first is based on the shape of the annual average NDVI or brightness-temperature profile, which was then approximated by a Fourier series. The coefficients estimated by the weighted least-squares method were used for classification. The second and third features were based on the raw periodogram of the time series and the auto-regressive modelling. A global land-cover training database created from Landsat Thematic Mapper and Multi-spectral Scanner imagery was used for training and validation. Both quadrature discriminate analysis (QDA) and linear discriminate analysis (LDA) were explored for classification, and results indicate that QDA performs much better than LDA. The first feature, based on the mean annual shape, produced much better results than the other two features. It was also found that NDVI signals worked better than brightness-temperature signals. That is probably because top-of-atmosphere signals were used, and atmospheric contaminations significantly disturb the thermal signals and correlation structures of different cover types. Further validations are needed.

1. Introduction

Land-cover maps are needed for global climate and ecosystem process models, as well as to characterize the distribution and status of major land surface types for environmental and ecological applications. Because of the temporal dynamics and changes in land surface, remote sensing is the only practical means for monitoring land-cover changes.

Different global, continental and regional land-cover datasets have been derived from remotely sensed data, particularly from Advanced Very High Resolution Radiometer (AVHRR) data, using various methods (Tucker *et al.* 1985, 1991, Malingreau 1986, Malingreau *et al.* 1989, Loveland *et al.* 1991, Loveland and Belward 1997, Townshend *et al.* 1991, Townshend 1994, DeFries *et al.* 1995, Cihlar *et al.* 1996, Nemani and Running 1997, Gopal *et al.* 1999). Because AVHRR has relatively coarse spectral and spatial resolution, most studies have utilized its multi-temporal characteristics to classify land cover. However, multi-year characteristics of AVHRR data

International Journal of Remote Sensing
ISSN 0143-1161 print/ISSN 1366-5901 online
http://www.tandf.co.uk/journals

have not been fully exploited. Data from AVHRR sensors have been acquired since 1981 and are expected to continue. The long temporal history is a very useful source to characterize land surface cover types, but it also requires advanced techniques to extract useful information. There exist numerous time series analysis techniques in the literature (e.g. Brockwell and Davis 1987), and several techniques have been explored to classify land-cover types using AVHRR data, such as Fourier analysis (Andres *et al.* 1994), change-vector analysis (Malila 1980, Lambin and Strahler 1994), principal component analysis (Anyamba and Eastman 1996) and others (e.g. Nemani and Running 1997), but few studies have taken direct and full advantage of the multi-year properties of AVHRR data.

Land-cover classification accuracy depends on many different factors, of which the effective features and the classification method are critical. Different land-cover classification algorithms have been explored in the literature, but the determination of effective features is still far from mature. Because of serious atmospheric contamination, the original two bands in the visible and near-infrared spectrum can not be used for effective features. Instead, vegetation indices such as normalized difference vegetation index (NDVI) have been widely used for global land-cover monitoring. Determining characteristic features from multi-temporal NDVI analysis and other AVHRR band combinations for global land-cover classification is still a challenging topic.

The present study focused on deriving the effective features for classifying global land-cover types using the monthly composite NOAA/NASA Pathfinder AVHRR Land data. Three types of features were explored. The first was based on the shape of the annual mean profile of the multi-year signals (NDVI or brightness temperature), which was approximated by a truncated third-order Fourier series. The coefficients estimated by the weighted least-squares method constituted the first type of feature. The second was the subset of the raw periodogram of the multi-year signals. The last was based on the auto-regressive (AR) model whose coefficients were used for classification.

A training database of 13 cover types for global land-cover classification has been created (DeFries *et al.* 1998). These pixels were extracted from the monthly composite dataset. One-half of these pixels were used for training and the other half for validation. Both quadrature discriminate analysis (QDA) and linear discriminate analysis (LDA) were used.

2. Datasets

The AVHRR sensor has five bands, one in red, one in near-infrared, one in mid-infrared and two in thermal-infrared. Its spatial resolution varies from 1.1 km at sub-nadir to more than 10 km off-nadir. More detailed characterizations can be found in many textbooks (e.g. Cracknell 1997).

NOAA/NASA-sponsored AVHRR Land Pathfinder dataset has been created to act as a precursor for the international Earth Observing Systems (EOS). In the Pathfinder AVHRR Land data, attempts have been made to eliminate some factors (James and Kalluri 1994). For example, Rayleigh scattering and ozone absorption have been corrected. All five original channels have been calibrated using the post-launch calibration algorithms. All pixels are accurately navigated and solar and scan angles are provided. The spatial resolution of all pixels have been normalized to be 8 km. The 12-year corrected, monthly composite dataset from 1982 to 1993 were used in this study.

A training database of global land cover has been compiled based on high-spatial resolution remotely sensed imagery and ancillary data (DeFries *et al.* 1998). A total of 169 Landsat scenes, mostly from the Multispectral Scanner system (MSS) was used to identify over 9000 pixels in the Pathfinder 8 km resolution data where there is high confidence that the labelled cover type occurs. A total of 13 cover types (table 1) from the original database (DeFries *et al.* 1998) were considered in this study.

3. Algorithm descriptions

The algorithms for extracting three types of features are discussed below. The coefficients of these models were input to classifiers for discriminating different cover types.

3.1. *Weighted least-squares method*

This approach consisted of two major steps. The first was to generate a mean annual profile. Because of the presence of noisy pixels, the median value over 12 years was used as the average. Mathematically,

$$L_j^{\mathrm{M}} = \text{median } (L_{j1}, L_{j2}, \dots L_{j12}) \tag{1}$$

where L_j^{M} denotes the monthly averaged observations from January ($j=1$) to December ($j=12$).

The second step was to approximate the annual mean profile by a truncated low-order Fourier series:

$$L_{\mathrm{j}}^{\mathrm{M}} = \sum_{i=1}^{I} [a_i \cos(i\phi_j) + b_i \sin(i\phi_j)] \tag{2}$$

a_i and b_i are Fourier coefficients. The phase term is defined as

$$\phi_j = 2\pi(j-1)/n$$

where $n=12$ represents 12 months and j ranges from 1 to n. After some initial experiments, it was found that $I=3$ is a good choice; thus, there were seven coefficients to be estimated.

An ordinary least-squares procedure can be used to estimate these Fourier coefficients. However, the fitted function may not represent the real seasonal trend

Table 1. Land-cover types and the training pixels.

	Cover types	Number of pixels
Cover 1	Evergreen needleleaf forests	386
Cover 2	Evergreen broadleaf forests	1181
Cover 3	Deciduous needleleaf forests	42
Cover 4	Deciduous broadleaf forests	353
Cover 5	Mixed forests	464
Cover 6	Woodlands	362
Cover 7	Wooded grasslands-shrubland	117
Cover 8	Closed bushlands or shrubland	237
Cover 9	Open shrubland	548
Cover 10	Grasslands	1098
Cover 11	Croplands	1379
Cover 12	Barelands	1196
Cover 13	Mosses and lichens	102

of the signals (NDVI and brightness temperature) very well. The reason is that the fitting considers all high and low values and the low NDVI or brightness-temperature values may result from atmospheric disturbance and other factors (Holben 1986). Instead, a weighted least-squares technique is applied. This is a two-step procedure. First, an ordinary least squares was implemented. Each point that deviates either positively or negatively from the fitted trend was assigned with a different weight. Negative deviations receive low weights, whereas positive deviations obtain high weights. In the second step, a weighted least-squares procedure was carried out. The weights were determined form the following formula (Sellers *et al.* 1996):

$$w_i = \begin{cases} 0 & U_i \leqslant -2 \\ [1+(U_i+r)/2]^4 & -2 < U_i < -r \\ 1 & -r < U_i < r \\ [1+(U_i-r)/2]^2 & U_i > r \end{cases} \tag{3}$$

where $U = (L^{\mathrm{M}} - \hat{L}^{\mathrm{M}})/A$, $\hat{L}^{\mathrm{M}}$ is the fitted L^{M} values based on the ordinary least-squares method (in step one); A is the median of the absolute difference of $\hat{L}^{\mathrm{M}}$ and L^{M}, i.e. $A = \text{median } \{|\hat{L}_i^{\mathrm{M}} - L_i^{\mathrm{M}}|\}$; and $r = A/20$.

3.2. *Periodogram*

Given a time series X_t where $t = 1, \ldots 144$ in this study, the auto-covariance C_t can be estimated (Venables and Ripley 1994):

$$C_t = \frac{1}{n} \sum_{s=min(1,\,-t)}^{s=max(n-t,\,n)} (X_{s+t} - \bar{X})(X_s - \bar{X}) \tag{4}$$

The periodogram $I(\omega)$ at frequency ω is the Fourier transformation of the auto-covariance:

$$I(\omega) = \sum_{-\infty}^{\infty} C_t \exp(-i\omega t) \tag{5}$$

It can be estimated by the following formula:

$$I(\omega) = \frac{1}{n} \left| \sum_{t=1}^{n} \exp(-i\omega t) X_t \right|^2 = \frac{1}{n} \left[\left\{ \sum_{t=1}^{n} X_t \sin(\omega t) \right\}^2 + \left\{ \sum_{t=1}^{n} X_t \cos(\omega t) \right\}^2 \right] \tag{6}$$

3.3. *Auto-regressive model*

An AR process of order p is defined by

$$X_t = \sum_{i=1}^{p} \alpha_i X_{t-i} + \varepsilon_t \tag{7}$$

where ε_t is the error term and α_i are coefficients. It is the special case of a more general model—the auto-regressive integrated moving average (ARIMA) model. An $ARIMA(p, d, q)$ model defines a process whose dth difference is a combination of the AR(p) and a qth order moving average (MA) model MA(q). Since the NDVI or brightness-temperature values of most cover types have significant seasonal variations, a seasonal version of the $ARIMA(p, d, q)$ model was used in this study to define AR models of both seasonal and non-seasonal components (Venables and Ripley 1994). After some experiments, it was found that an ARIMA $((2,0,0) \times (4,0,0)_{12})$ provided reasonably good summaries of the NDVI or brightness-temperature signals, where the seasonal term was modelled as AR(4), the non-seasonal term was modelled as AR(2) and the number 12 indicates the period of 12 months for the differencing process.

4. Land-cover classification results and analysis

4.1. *Weighted least-squares method*

The average annual profiles of NDVI and channel 4 brightness temperature of all 13 cover types are displayed in figure 1. The NOAA/NASA Pathfinder data keep only observations with the solar zenith angle smaller than 70°. Some cover types distributed in the high-latitude regions may have many missing pixels in the winter seasons, which corresponds to the channel 4 brightness temperature as low as 160° in this figure. In the winter of 1988, NOAA9 reached the end of its lifetime. Because of satellite orbital drifts (McGregor and Gorman 1994, Privette *et al.* 1995, Roderick *et al.* 1996), the solar zenith angle is very low in the winter so that many cover types do not have any observations during that period of time.

It is also noticed that the NDVI values increased in general from the 1980s to the 1990s, but the channel 4 brightness temperatures of NOAA7, 9 or 11 decreased. It was found that this is primarily the result of satellite orbital drifts. It may be a serious problem for studies on surface change detection, but it does not significantly affect land-cover classification.

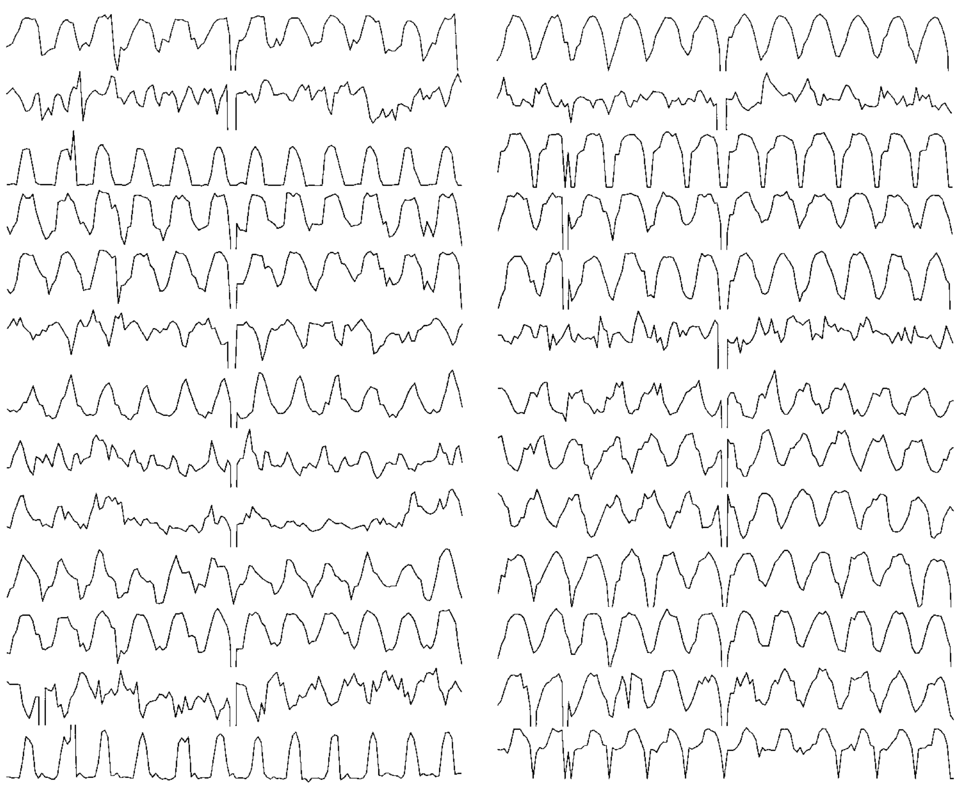

Figure 1. Twelve-year (1982–1993) average profiles of NDVI and band 4 brightness temperatures of 13 cover types. The first column represents the NDVI profiles, and the second represents the profiles of AVHRR band 4 brightness temperature. The 13 rows correspond to 13 cover types, which are defined in table 1.

In spite of the problems discussed above, it can still clearly be seen that different cover types have unique NDVI or brightness temperature profiles. This forms the basis for distinguishing them and using them as classification inputs.

Land-cover classification based on the NDVI annual 'shape' has been reported in the literature (e.g. DeFries *et al.* 1995). Because the surface NDVI or temperature profiles are so easily contaminated by sub-pixel clouds or other factors, it is advantageous to classify them based on the mean annual profiles from multi-year signals.

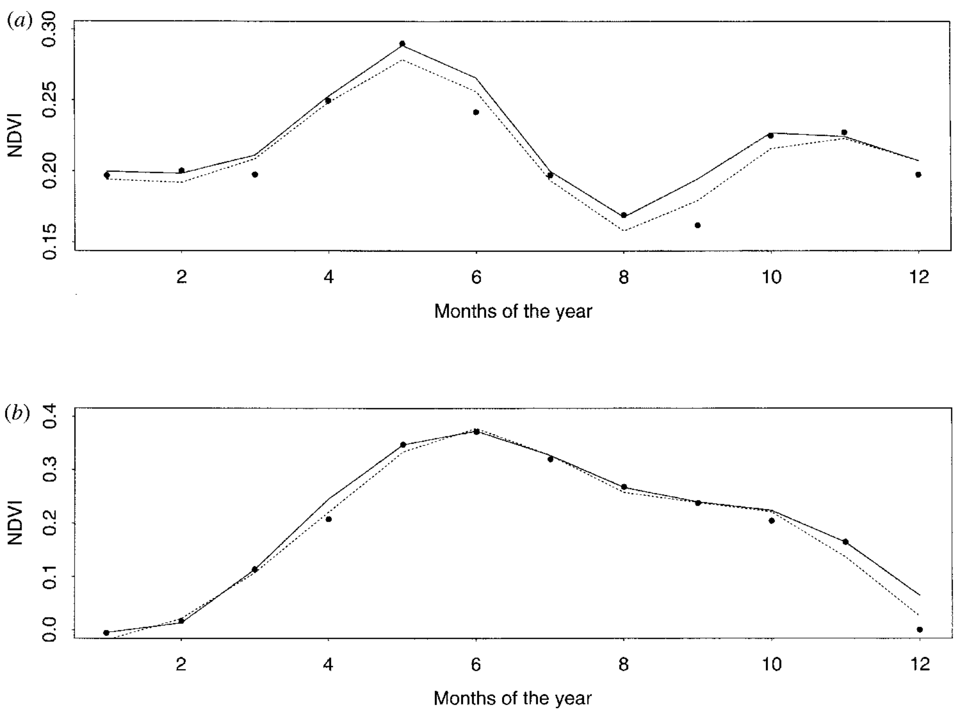

Figure 2. Illustration of the third-order Fourier series approximations to these two NDVI average annual profiles using both the ordinary least-squares method (solid lines) and the weighted least-squares method (dashed lines).

Table 2. Coefficients of the weighted least-squares fitting that is shown in figure 2.

	Coefficients						
Cover type	a_0	a_1	b_1	a_2	b_2	a_3	b_3
Closed bushlands or shrubland	0.2130	-0.0042	0.0246	-0.0191	-0.0329	0.0045	0.0084
Grasslands	0.1873	-0.1699	0.0190	-0.0336	-0.0358	-0.0031	0.0195

Two examples are shown in figure 2. The monthly NDVI values are the median values of the corresponding methods in the period of 12 years. Both the ordinary least-squares method and the weighted least-squares method produce similar fittings. The coefficients using the weighted least-squares method are presented in table 2. Both fittings are good, indicating that the third-order Fourier series is sufficient to summarize the variations. It is also obvious that the weighted least-squares method generated the higher r^2 values. The major difference is that the curves fitted by the weighted least-squares method constitute the upper bounds of these NDVI points.

The classification results based on the weighted least-squares method are summarized in table 3. It is clear that QDA is much better than LDA and that the NDVI features are better than the channel 4 brightness temperature. The best result was achieved when both NDVI and channel 4 coefficients were combined into classifiers in which both surface reflective and emitted properties were utilized. This result is consistent with the earlier reports (e.g. Nemani and Running 1997). When all 14 coefficients were input into the classifiers, cover type 3 did not have enough samples necessary for training. Therefore, this cover type was excluded when using all 14 coefficients. The detailed misclassification matrices are presented in table 4. Notice that these matrices are not symmetrical. When the classification is based on the channel 4 brightness temperature (table 4(*b*)), cover type 6 (woodlands) is the poorest classified, with a classification accuracy of 40.1%, followed by cover type 1 (evergreen needleleaf forests) with 60.1%. If the feature is based on NDVI (table 4(*a*)), cover type 7 (wooded grasslands-shrubland) has the lowest classification accuracy of 71.8%, followed by cover type 1 with 77.2% and cover type 6 with 82.3%. If both NDVI and channel 4 brightness temperature are used as features (table 4(*c*)), cover type 8 (closed bushlands or shrubland) has the lowest classification accuracy of 88.6%, followed by cover type 7 of 88.9% and cover type 6 of 90.1%. These cover types (e.g. 6 and 7) are more difficult to distinguish from grasslands and croplands.

4.2. *Periodogram*

The raw periodogram of all 13 cover types is shown in figure 3. The plots are on a log scale, in units of *decibels*, i.e. the plot is of $10\log_{10}I(\omega)$. Different cover types obviously display different patterns of the raw periodogram. Particularly noticeable is the peak at the frequency 1 (lag 12) when the signal has a regular seasonal pattern.

It is necessary to determine the feature from the raw periodogram for classification. To select the same number of inputs from the raw periodogram as in the weighted least-squares method, periodogram values were arbitrarily selected at lags

Table 3. Overall classification accuracy (%) based on the weighted least-squares method with two classifiers and three classification features (T4 represents band 4 brightness temperature).

Classifier	Feature: NDVI	Feature: T4	Feature: NDVI+T4
LDA	75.58	64.59	81.07
QDA	91.17	84.15	95.89

Table 4. Classification matrix using the weighted least-squares method with (a) the NDVI feature, (b) band 4 brightness temperature feature and (c) the combined NDVI and band 4 brightness temperature feature.

(a)	Cover types												
Cover types	1	2	3	4	5	6	7	8	9	10	11	12	13
1	149	23	0	3	7	8	0	0	0	0	3	0	0
2	1	566	0	3	8	5	0	0	0	0	7	0	0
3	0	0	21	0	0	0	0	0	0	0	0	0	0
4	3	7	0	161	5	1	0	0	0	0	0	0	0
5	13	4	0	1	208	2	0	0	0	0	4	0	0
6	17	4	0	3	1	149	0	0	0	0	7	0	0
7	0	0	0	0	0	3	42	1	0	3	9	0	0
8	0	0	0	0	0	0	7	98	2	11	1	0	0
9	0	0	0	0	0	0	0	2	258	14	0	0	0
10	0	0	0	1	0	9	2	0	31	477	29	0	0
11	0	19	0	3	4	20	2	0	0	9	632	0	0
12	0	0	0	0	0	0	0	0	0	1	0	597	0
13	0	0	0	0	0	0	0	0	0	0	6	0	45

(b)	Cover types												
Cover types	1	2	3	4	5	6	7	8	9	10	11	12	13
1	116	0	0	5	33	10	0	0	0	2	27	0	0
2	0	565	0	1	0	2	0	0	11	0	11	0	0
3	0	0	21	0	0	0	0	0	0	0	0	0	0
4	0	24	0	135	5	0	0	0	0	0	13	0	0
5	1	0	0	2	190	2	0	0	4	0	33	0	0
6	4	12	3	10	0	74	2	15	13	18	25	0	5
7	0	0	0	0	0	2	41	1	4	8	2	0	0
8	0	0	0	0	0	0	9	86	18	3	3	0	0
9	0	0	0	0	0	0	7	6	237	17	7	0	0
10	5	3	0	1	12	4	6	0	3	427	88	0	0
11	1	8	0	5	7	7	4	4	28	21	604	0	0
12	0	0	0	0	0	0	0	0	1	3	0	594	0
13	0	0	0	0	0	0	0	0	0	0	0	0	51

(c)	Cover types											
Cover types	1	2	4	5	6	7	8	9	10	11	12	13
1	180	4	0	5	2	0	0	0	0	2	0	0
2	0	577	4	0	2	0	0	0	0	0	7	0
4	0	11	164	1	0	0	0	0	0	1	0	0
5	8	0	1	217	0	0	0	0	0	6	0	0
6	5	1	3	0	163	3	0	0	0	6	0	0
7	0	0	0	0	1	52	0	0	2	3	0	0
8	0	0	0	0	0	7	105	0	6	1	0	0
9	0	0	0	0	0	0	1	263	8	2	0	0
10	0	0	1	0	3	1	0	2	525	17	0	0
11	1	0	0	2	3	0	0	0	15	668	0	0
12	0	0	0	0	0	0	0	0	4	0	594	0
13	0	0	0	0	0	0	0	0	0	0	0	51

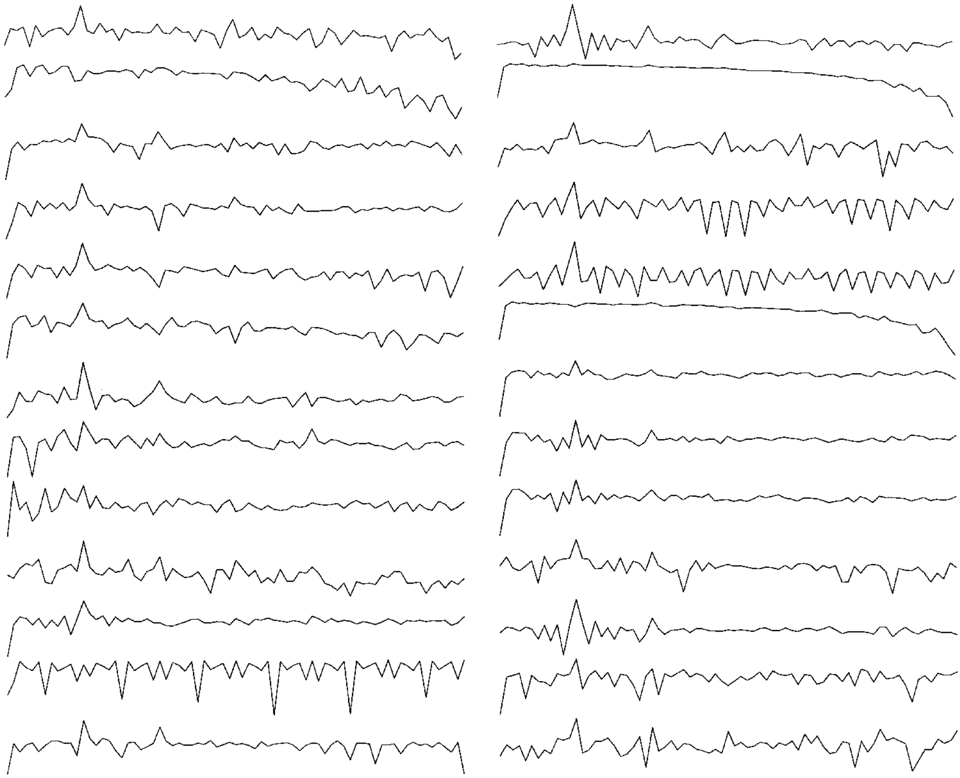

Figure 3. Raw periodogram of NDVI and channel 4 brightness temperatures of 13 cover types. The plots are on a log scale, in units of *decibels*, i.e. $10\log_{10}I(\omega)$. The first column represents NDVI, and the second represents band 4 brightness temperature. The 13 rows correspond to 13 cover types, which are defined in table 1.

of 6, 8, 10, 12, 14 and 26, corresponding to frequencies of 0.5, 0.67, 0.83, 1 and 2.17 and the median value of the signal for classification.

Since it has been demonstrated above that QDA works better than LDA, only QDA was used in the rest of this study. The total of seven inputs of the NDVI raw periodogram generated an overall classification accuracy of 83.34%. When the same procedure was applied to the channel 4 brightness temperature, the overall classification accuracy was 76.97%. If both features (14 inputs) were combined without cover type 3, the overall classification accuracy was 91.96%.

To find out whether the optimal choice of the subset of the raw periodogram will produce the better classification results, both the within-group variance and the between-group variance were calculated. To maximize the cover type discrimination, it was necessary to select the features so that the within-group variance should be as small as possible and the between-group variance as large as possible. Instead of using the individual variance, the common practice is to use the ratio of the between-group variance to the within-group variance. The larger the ratio, the better for cover-type discrimination. These two types of variances, and their ratio of the NDVI raw periodogram at lags smaller than 50, are displayed in figure 4. It seems the mean NDVI is the most useful feature, since the ratio of the between-group variance to the within-group variance is the largest. Another remarkable peak of the variance ratio is at lags around 12. The raw periodogram at lags around 12 characterizes the annual shape of the NDVI profile. It explains why the weighted least-squares method, based on the annual shape of the NDVI profile, can produce very good classification results, as demonstrated in the previous section.

According to the magnitude of the ratio, the first seven best raw periodograms at lags of 1, 13, 12, 19, 25, 37 and 14 were selected. The classification accuracy was 83%, which was not significantly better than the previous classification results. When the first 14 best features were chosen at lags of 1, 13, 12, 19, 25, 37, 14, 18, 7, 31, 44, 4, 6, 43, the classification accuracy became 87.46%. It seems that the better choice of the subset of the raw periodogram does not improve the classification results significantly.

4.3. *Auto-regressive model*

The auto-correlation coefficients of the different cover types are shown in figure 5. Dashed lines indicate the approximate 95% confidence limits. It can be seen that the NDVI and brightness temperature of covers 8, 9 and 12 did not show any significant correlation 'structures'.

In the initial analysis, AR(7) and AR(14) models were fitted to the NDVI values of each pixel. The overall classification accuracy was 62.18% and 73.72%, respectively.

In the attempt to improve classification results, an ARIMA $((2,0,0)\times(4,0,0)_{12})$ was fitted to the NDVI signal, the classification accuracy using these six coefficients and the median NDVI value was 68.83%. It was an improvement when compared to the AR(7) model, but it was still not as good as the classification results using the weighted least-squares method or the raw periodogram. Very similar results were achieved from the channel 4 brightness temperature.

These results indicate that the correlation structures of the multi-year signals (NDVI or channel 4 brightness temperature) are not very effective for land-cover classification. One of the main reasons is probably that the monthly composite data still contain a great deal of cloudy or sub-cloudy pixels, which greatly impact the correlation 'structure' of the remotely sensed data of different cover types.

5. Conclusions

Multi-temporal AVHRR data have been used for characterizing land surface cover types in many studies, but multi-year characteristics of AVHRR data have not been fully exploited. One of the challenging issues is to derive effective features as inputs to classifiers.

To achieve higher classification accuracy of global land cover using the multi-year NOAA/NASA Pathfinder AVHRR Land data, techniques were explored to extract three types of features and input them into two classifiers. The first feature was based on the shape of the annual average NDVI and channel 4 brightness temperature profiles. A weighted least-squares method was then used to approximate the average annual profile, and the estimated coefficients were used for classification.

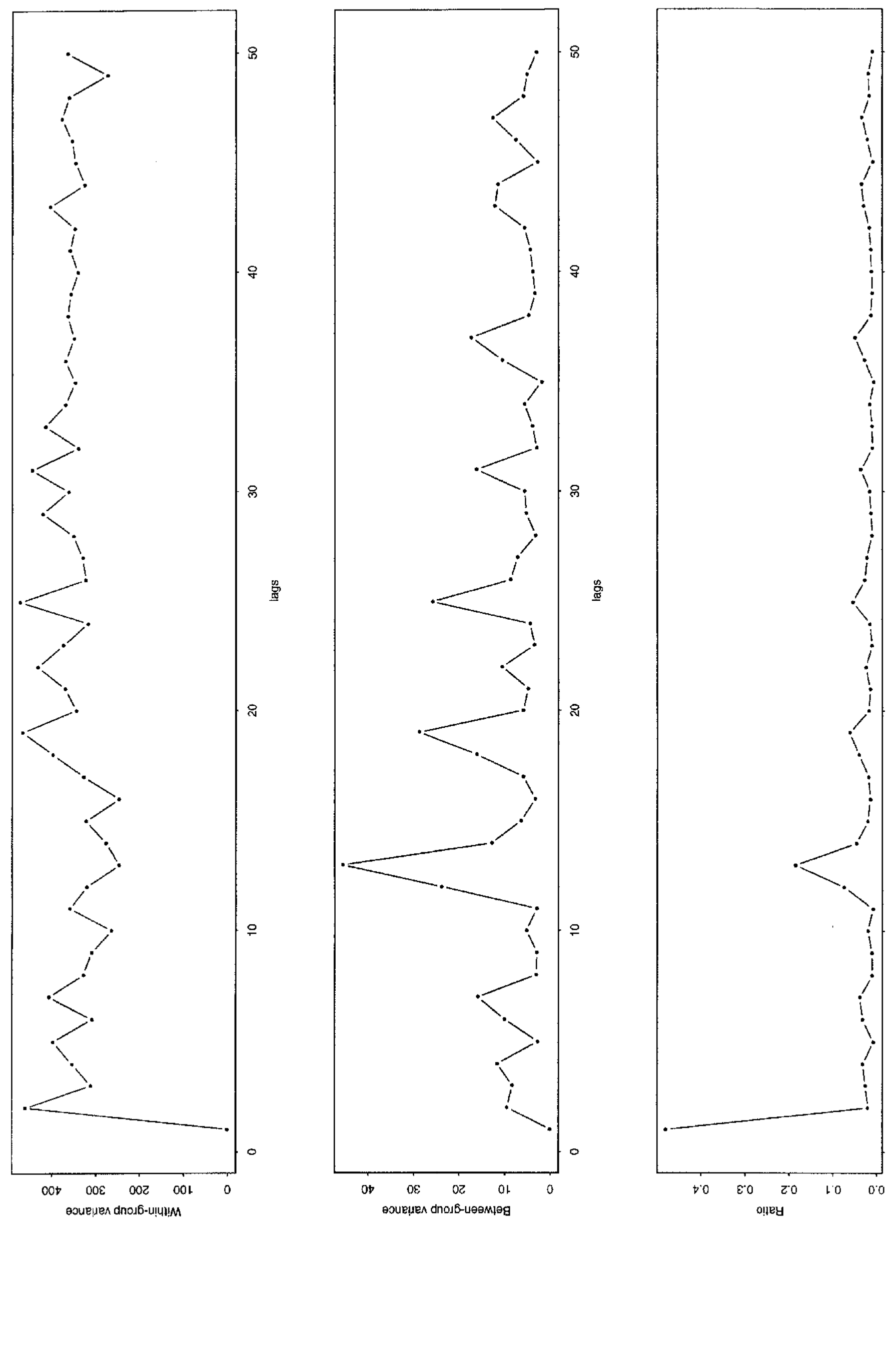

Figure 4. Within-group variance and between-group variance of the NDVI raw periodogram, and the ratio of the between-group variance and within-group variance for determining the best features for classification.

The second feature was based on the raw periodogram of the multi-year signals. The subset of the raw periodogram for each pixel was then used for classification. The third feature was based on the correlation structure of the temporal signal. An AR model and the seasonal ARIMA model were fitted to the temporal signals, and the coefficients were used for classification.

Based on training data that were created from Landsat TM and MSS imagery, the weighted least-squares method, using the annual average temporal profiles, generated the best classification results. Additionally, the NDVI features were better than the channel 4 brightness temperature features. It is consistent with the earlier studies that NDVI was less sensitive to atmosphere contamination than a single thermal band. If land surface temperature, that may be estimated from the split-window algorithms or other techniques, were input into classifiers, the conclusion may have been different. However, since land surface temperature estimation algorithms from AVHRR data are still in the research stage, no attempts were made to integrate them in this study. When two sets of coefficients from both NDVI and band 4 brightness temperature were combined, the best overall classification accuracy of 95.9% was obtained. The classification results based on the raw periodogram and the correlation structure were not as good as those based on the annual average profile. One of the reasons is probably because these two types of features are highly sensitive to contaminated pixels. Cloudy or sub-pixel cloudy pixels significantly disturb the unique periodogram and correlation structure of each cover type. In this study, every individual observation was used, no matter whether it was labelled as a cloudy pixel, mixed pixel or bad-quality pixel. If satellite data can be effectively corrected atmospherically, these two approaches, based on the raw periodogram and the correlation structure, will probably be a very powerful way to classify land-cover types.

Two classifiers (QDA and LDA) were used in this study. QDA consistently produced the better classification results, indicating that the boundaries of different cover types in the feature space are not linear in general. It showed that the determination of classification features is critical, but the choice of a classifier is also important.

This study focused on the NOAA/NASA Pathfinder AVHRR data, but the basic procedures can be used for any temporal profiles of remotely sensed data. In particular, these methods might be helpful to analyse Moderate Resolution Imaging Spectroradiometer (MODIS) data in the EOS era.

Acknowledgments

The author would like to thank Dr Ruth DeFries, for her review of this manuscript and her kind assistance in processing the global land-cover training dataset. The author also wishes to acknowledge anonymous reviewers and the editor for their constructive comments and help.

Figure 5. Auto-correlation plots of NDVI and channel 4 brightness temperatures of 13 cover types defined in table 1. Dashed lines indicate the approximate 95% confidence limits. The first column represents NDVI, and the second represents band 4 brightness temperature; (*a*) represents the first six cover types, and (*b*) represents the last seven cover types.

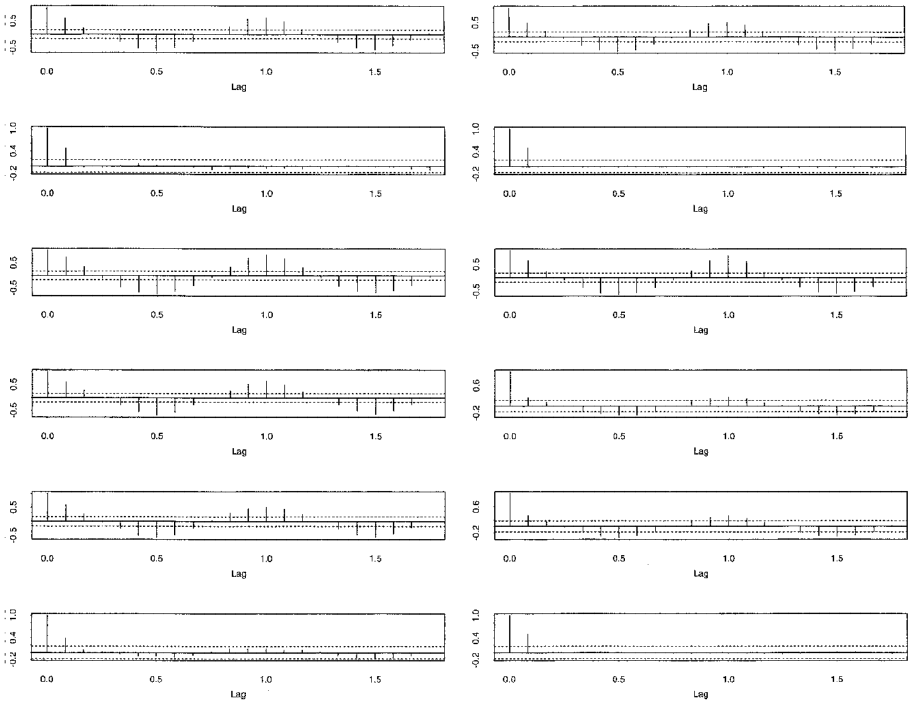

(*a*)

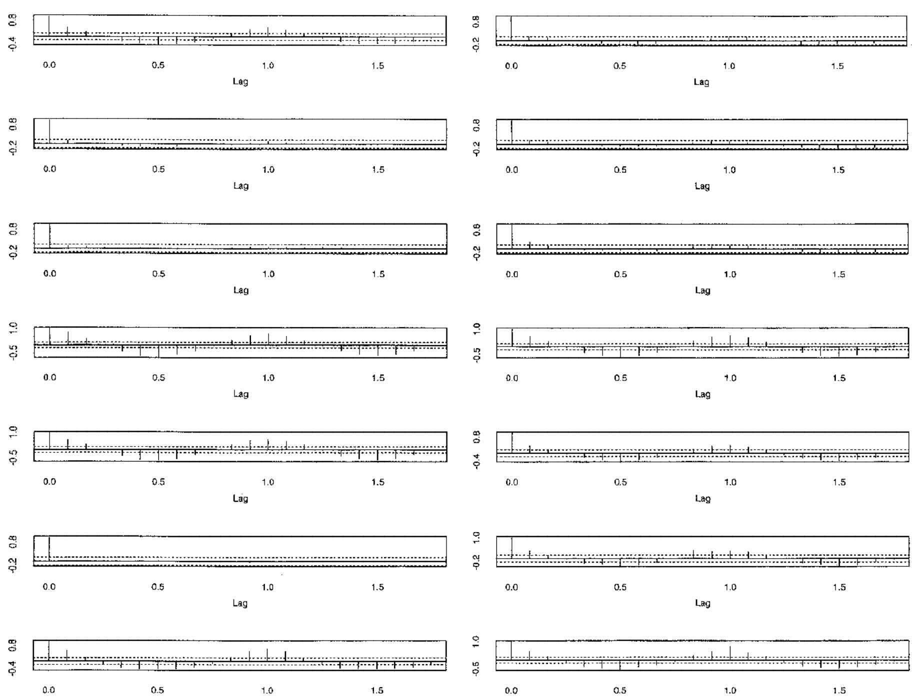

(*b*)

References

Andres, L., Salas, W. A., and Skole, D., 1994, Fourier analysis of multi-temporal AVHRR data applied to a land cover classification. *International Journal of Remote Sensing*, **15**, 1115–1121.

Anyamba, A., and Eastman, J. R., 1996, Interannual variability of NDVI over Africa and its relation to El Nino/Southern Oscillation. *International Journal of Remote Sensing*, **17**, 2533–2548.

Brockwell, P. J., and Davis, R. A., 1987, *Time Series: theory and methods* (New York: Springer-Verlag).

Cihlar, J., Hung, L., and Xiao, Q., 1996, Land cover classification with AVHRR multichannel composites in northern environments. *Remote Sensing of Environment*, **58**, 36–51.

Cracknell, A. P., 1997, *The Advanced Very High Resolution Radiometer* (London: Taylor & Francis).

DeFries, R., Hansen, M., and Townshend, J., 1995, Global discrimination of land cover types from matrices derived from AVHRR Pathfinder Data. *Remote Sensing of Environment*, **54**, 209–222.

DeFries, R., Hansen, M., Townshend, J., and Sohlberg, R., 1998, Global land cover classifications at 8 km spatial resolution. Part 1: Training and validation data derived from Landsat imagery. *International Journal of Remote Sensing*, **19**, 3141–3168.

Gopal, S., Woodcock, C. E., and Strahler, A. H., 1999, Fuzzy neural network classification of global land cover from a 1 degree AVHRR data set. *Remote Sensing of Environment*, **67**, 230–243.

Holben, B. N., 1986, Characteristics of maximum-value composite images from temporal AVHRR data. *International Journal of Remote Sensing*, **7**, 1417–1434.

James, M. E., and Kalluri, S., 1994, The Pathfinder AVHRR land data set: an improved coarse resolution data set for terrestrial monitoring. *International Journal of Remote Sensing*, **15**, 3347–3364.

Lambin, E. F., and Strahler, A. H., 1994, Change-vector analysis in multitemporal space: a tool to detect and categorize land-cover change processes using high temporal-resolution satellite data. *Remote Sensing of Environment*, **48**, 231–244.

Loveland, T. R., and Belward, A. S., 1997, The IGBP-DIS global 1 km land cover data set, DISCover: first result. *International Journal of Remote Sensing*, **18**, 3289–3296.

Loveland, T. R., Merchant, J. W., Ohlen, D. O., and Brown, J. F., 1991, Development of a land-cover characteristics database for continuous U.S. *Photogrammetry Engineering and Remote Sensing*, **57**, 1453–1463.

Malila, W. A., 1980, Change vector analysis: an approach for detecting forest changes with Landsat. *Proceedings of the 6th Annual Symposium on Machine Processing of Remotely Sensed Data, Purdue University, West Lafayette, Indiana, 3–6 June 1980*, pp. 326–335.

Malingreau, J. P., 1986, Global vegetation dynamics: satellite observations over Asia. *International Journal of Remote Sensing*, **7**, 1121–1146.

Malingreau, J.-P., Tucker, C. J., and Laporte, N., 1989, AVHRR for monitoring global tropical deforestion. *International Journal of Remote Sensing*, **10**, 855–867.

McGregor, J., and Gorman, A. J., 1994, Some considerations for using AVHRR data in climatological studies: I. Oribital characteristics of NOAA satellites. *International Journal of Remote Sensing*, **15**, 537–548.

Nemani, R., and Running, S., 1997, Land cover characterization using multitemporal red, near-IR, and thermal-IR data from NOAA/AVHRR. *Ecological Applications*, **7**, 79–90.

Privette, J. L., Fowler, C., Wick, G. A., Baldwin, D., and Emery, W. J., 1995, Effects of orbital drift on advanced very high resolution radiometer products: normalized difference vegetation index and sea surface temperature. *Remote Sensing of Environment*, **53**, 164–171.

Roderick, M., Smith, R., and Lodwick, G., 1996, Calibrating long-term AVRHH-derived NDVI imagery. *Remote Sensing of Environment*, **58**, 1–12.

Sellers, P. J., Sietse, S. O., Tucker, C. J., Justice, C. O., Dazlich, D. A., Collatz, G. J., and Randall, D. A., 1996, A revised land surface parameterization (SiB2) for Atmospheric GCMs. Part II: The generation of global fields of terrestrial biophysical parameters from satellite data. *Journal of Climate*, **9**, 706–737.

Townshend, J. G. R., 1994, Global data sets for land applications from the Advanced Very High Resolution Radiometer: an introduction. *International Journal of Remote Sensing*, **15**, 3319–3332.

Townshend, J. R. G., Justice, C. O., Li, W., Gurney, C., and McManus, J., 1991, Global land cover classification by remote sensing: present capabilities and future possibilities. *Remote Sensing of Environment*, **35**, 243–255.

Tucker, C. J., Townshend, J. R. G., and Goff, T. E., 1985, African land-cover classification using satellite data. *Science*, **227**, 369–375.

Tucker, C. J., Dregne, H. E., and Newcomb, W. W., 1991, Expansion and contraction of the Sahara Desert from 1980 to 1990. *Science*, **253**, 299–301.

Venables, W. N., and Ripley, B. D., 1994, *Modern Applied Statistics with S-Plus* (New York: Springer-Verlag).